

DOI: <https://doi.org/10.17816/DD76511>

Наблюдения доплеровского мерцающего артефакта: база данных радиочастотных ультразвуковых сигналов

Д.В. Леонов^{1, 2}, Р.В. Решетников^{1, 3}, Н.С. Кульберг^{1, 4}, А.А. Насибуллина², А.И. Громов⁵

¹ Научно-практический клинический центр диагностики и телемедицинских технологий Департамента здравоохранения г. Москвы, Москва, Российская Федерация

² Национальный исследовательский университет МЭИ, Москва, Российская Федерация

³ Первый Московский государственный медицинский университет имени И.М. Сеченова (Сеченовский Университет), Москва, Российская Федерация

⁴ Федеральный исследовательский центр «Информатика и управление» Российской академии наук, Москва, Российская Федерация

⁵ Московский государственный медико-стоматологический университет имени А.И. Евдокимова, Москва, Российская Федерация

АННОТАЦИЯ

Обоснование. Мерцающий артефакт в доплеровских режимах ультразвукового исследования проявляется быстрой хаотической сменой окрашенных пикселей на экране прибора. Явление, которое можно использовать в качестве полезного диагностического признака, исследовано недостаточно. Большинство предположений о причинах артефакта сделаны на основании изображений с экрана ультразвукового прибора без глубокого изучения свойств принимаемых сигналов.

Материалы и методы. Радиочастотные ультразвуковые сигналы были записаны при исследовании фантомов. Исследовались как объекты, приводящие к появлению мерцающего артефакта на экране прибора, так и имитации сосудов и мягких тканей. Сбор данных проводился с июля 2016 по март 2021 г. Данные получены при помощи исследовательского ультразвукового прибора «Сономед-500» с датчиками 7,5 L38 и 3,4 С60.

Содержимое базы данных. Представлена база данных, содержащая радиочастотные сигналы, полученные с выхода формирователя луча из приёмного тракта ультразвукового медицинского диагностического прибора в режиме цветного доплеровского картирования и В-режиме. Представленные в базе данных сигналы содержат признаки мерцающего артефакта. База состоит из исследований пяти различных фантомов общим объёмом 10,5 ГБ. Радиочастотные данные сохранены в бинарном виде. Настройки сканирования, необходимые для анализа радиочастотных данных, содержатся в текстовых файлах. Каждое исследование сопровождается примером характерной сонограммы в графическом формате. База данных доступна по адресу: https://mosmed.ai/datasets/ultrasound_doppler_twinkling_artifact.

Доступность кода. Для просмотра и анализа базы данных к архиву прилагаем разработанную нами программу TwinklingDatasetDisplay. Доступен исходный код программы: <https://github.com/Center-of-Diagnostics-and-Telemedicine/TwinklingDatasetDisplay.git>.

Условия использования. База данных может быть использована для разработки и тестирования алгоритмов обработки ультразвуковых сигналов. Доступ к базе данных и коду для её просмотра открыт для всех желающих.

Ключевые слова: цветная ультразвуковая доплерография; мерцающий артефакт; база данных; «сырые» радиочастотные данные; ультразвуковые фантомы.

Как цитировать

Леонов Д.В., Решетников Р.В., Кульберг Н.С., Насибуллина А.А., Громов А.И. Наблюдения доплеровского мерцающего артефакта: база данных радиочастотных ультразвуковых сигналов // *Digital Diagnostics*. 2021. Т. 2, № 3. С. 261–276. DOI: <https://doi.org/10.17816/DD76511>

DOI: <https://doi.org/10.17816/DD76511>

Doppler twinkling artifact observations: an open-access database of raw ultrasonic signals

Denis V. Leonov^{1,2}, Roman V. Reshetnikov^{1,3}, Nikolay S. Kulberg^{1,4}, Anastasia A. Nasibullina², Alexandr I. Gromov⁵

¹ Moscow Center for Diagnostics and Telemedicine, Moscow, Russian Federation

² National Research University Moscow Power Engineering Institute, Moscow, Russian Federation

³ The First Sechenov Moscow State Medical University (Sechenov University), Moscow, Russian Federation

⁴ Federal Research Center Computer Science and Control of the Russian Academy of Sciences, Moscow, Russian Federation

⁵ Moscow State University of Medicine and Dentistry named after A.I. Evdokimov, Moscow, Russian Federation

ABSTRACT

BACKGROUND: Doppler twinkling artifact is a rapid change of colors seen in CFI-mode in the presence of kidney stones and calculi. Therefore, numerous researchers use the twinkling artifact as a diagnostic sign. However, this phenomenon is under-researched, because most assumptions concerning its causes are made based on pure visual observations of the scanner's screen leaving the important steps of signal transformation hidden behind the "black box" curtains of ultrasound machines.

MATERIALS AND METHODS: Raw radiofrequency ultrasound signals were recorded in the phantom studies. The recorded echoes were received from objects that create the Doppler twinkling artifact and artificial blood vessels and soft tissues imitators. The data were collected between June 2016 and March 2021. Sonomed-500 with the 7.5 L38 and 3.4 C60 probes served as the research machine for the signal capture.

Data records: We present the database containing raw radiofrequency ultrasound signals from the beam former output of the research ultrasound machine. The dataset consists of CFI and B-mode echoes recorded from twinkling objects. Therefore, this database can be useful for those who test, develop and study ultrasound signal processing algorithms. Furthermore, the database is freely available online. The 10.5 GB database consists of echoes received from five phantoms. Raw radiofrequency signals were stored in the binary files; scanning parameters were stored in text files. The database is available at: https://mosmed.ai/datasets/ultrasound_doppler_twinkling_artifact.

Code availability: The public can visualize the database content with the specially written program TwinklingDatasetDisplay available at: <https://github.com/Center-of-Diagnostics-and-Telemedicine/TwinklingDatasetDisplay.git>.

Usage notes: The database can be used to test and develop signal-processing algorithms, such as wall filtration, velocity estimation, feature extraction, speckle reduction, etc. Furthermore, the public is free to share (copy, distribute, and transmit) and remix (adapt and do derivative works) the dataset considering appropriate credit is given.

Keywords: ultrasonography; color flow imaging; Doppler twinkling artifact; dataset; raw radiofrequency signals; ultrasound phantoms.

To cite this article

Leonov DV, Reshetnikov RV, Kulberg NS, Nasibullina AA, Gromov AI. Doppler twinkling artifact observations: an open-access database of raw ultrasonic signals. *Digital Diagnostics*. 2021;2(3):261–276. DOI: <https://doi.org/10.17816/DD76511>

Received: 24.07.2021

Accepted: 24.08.2021

Published: 27.09.2021

DOI: <https://doi.org/10.17816/DD76511>

多普勒观测闪烁神器：射频超声信号数据库

Denis V. Leonov^{1,2}, Roman V. Reshetnikov^{1,3}, Nikolay S. Kulberg^{1,4},
Anastasia A. Nasibullina², Alexandr I. Gromov⁵

¹ Moscow Center for Diagnostics and Telemedicine, Moscow, Russian Federation

² National Research University Moscow Power Engineering Institute, Moscow, Russian Federation

³ The First Sechenov Moscow State Medical University (Sechenov University), Moscow, Russian Federation

⁴ Federal Research Center Computer Science and Control of the Russian Academy of Sciences, Moscow, Russian Federation

⁵ Moscow State University of Medicine and Dentistry named after A.I. Evdokimov, Moscow, Russian Federation

简评

论证。通过仪器筛网上涂漆像素的快速混乱变化，表现出多普勒模式中的闪烁伪影。不能足够地研究可用作有用的诊断特征的现象。关于工件的原因的大多数假设是基于来自超声波装置屏幕的图像而没有深入研究接收信号的性质的深度研究。

材料与方射频超声信号记录在幽灵的研究中。这些物体导致器件屏幕上的闪烁伪像以及血管和软组织的模仿。从2016年7月到3月2021年进行数据收集使用Sonad-500研究超声仪器获得数据，具有7, 5 L38和3, 4 C60传感器。

内容数据库 提供了一个包含射频信号的数据库，彩色多普勒成像模式下超声医学诊断仪接收通路波束形成器输出的结果和B-式。数据库中呈现的信号包含闪烁的伪影的符号。基础包括研究五种不同幽灵的研究，总体积为10.5 GB。射频数据以二进制形式存储。分析射频数据所需的扫描设置包含在文本文件中。每项研究伴随着以图形格式的特征超声图的示例。数据库可在以下网址查阅：https://mosmed.ai/datasets/ultrasound_doppler_twinkling_artifact。

代码可用性。为了查看和分析数据库，请将我们开发的TwinklingDataSetDisplay软件添加到存档中。程序源代码可用：<https://github.com/Center-of-Diagnostics-and-Telemedicine/TwinklingDatasetDisplay.git>。

使用条款。数据库可用于开发和测试用于处理超声信号的算法。访问数据库和用于查看它的代码为每个人都打开。

关键词：彩色超声波多普拉洛林；闪烁的神器；数据库；“原始”射频数据；超声波幻影。

引用本文

Leonov DV, Reshetnikov RV, Kulberg NS, Nasibullina AA, Gromov AI. 多普勒观测闪烁神器：射频超声信号数据库. *Digital Diagnostics*. 2021;2(3):261–276. DOI: <https://doi.org/10.17816/DD76511>

收到: 24.07.2021

接受: 24.08.2021

发布日期: 27.09.2021

BACKGROUND

A twinkling artifact in the color flow mapping (CFM) mode appears as a fast chaotic change of colored pixels on the screen of ultrasonic medical devices. This artifact is observed in the modes that were originally designed to assess blood flow, with marking of areas where blood motion is excluded. The clinical significance of the problem is related to the potential use of a twinkling artifact as an additional diagnostic sign when searching for stones in the kidney, ureter and bladder, and gallbladder and bile duct. Moreover, this artifact may be useful for detecting micro calcifications in breast neoplasms [1–8]. The high prevalence and social significance of these diseases and possible difficulties in their detection using traditional ultrasonic imaging require additional diagnostic options, such as the skillful use of the twinkling artifact. The detectability and intensity of the twinkling artifact varied and depend on the scanning equipment and its settings.

Several competing and weakly related hypotheses have tried to explain the cause of the twinkling artifact [9–16]. To prove their hypotheses, most authors have cited images from the screen of the ultrasonic device. The ultrasonic device was a “black box” for the authors of these hypotheses. Assumptions about the causes of the twinkling artifact were made without studying all signal processing steps. Thus, most hypotheses cannot be substantiated.

Unfortunately, the majority of available studies on the twinkling artifact did not analyze radiofrequency (RF) data, which carry more information compared with sonograms. Thus, hard-to-reach research instruments that provide access to raw RF signals are needed to obtain such data. Currently, no datasets exist in the public domain that contains ultrasonic Doppler signals with signs of the twinkling artifact.

This article presents an open-access database of RF signals, which were obtained from the beamformer output of the preprocessing path of a research ultrasonic device, and a tool for its viewing and analysis.

METHODS

Eligibility criteria

The database contains RF signals of observations of artificial objects (phantoms) that contain signs of the twinkling artifact. Only after the appearance of the stable twinkling artifact on two ultrasound machines was achieved, the corresponding signals were included in the database. The database also includes records of a blood mimicking fluid from a Doppler flow phantom, which imitates the normal blood flow in the vessel.

Data collection

The study was conducted between July 2016 and July 2021.

Ultrasonic equipment

Data were obtained from the CFI- and B-mode channels of the Sonomed-500 ultrasonic device (Spectromed, Moscow) by using linear (7.5 L38) and convex (3.4 C60) transducers.

RF signals from which the database was formed are shown in Fig. 1. The 64 elements of the phased array transducer were used to form a beam for each scanning direction. At the transmission stage, all selected elements emit pulses with specific delays to focus ultrasound at a predetermined depth. Pulses of approximately 1 μ s and 4 μ s duration for the B-mode and Doppler mode, respectively, were emitted. Echoes were received separately by each array element, further amplified in an analog receiver module, and digitized at a frequency of 50 MHz. Digital signals of individual channels were coherently summarized in the beamformer with delays that provide dynamic focusing. Each signal or the formed beam was subjected to decimation, that is, the frequency of digitization was reduced to 10 MHz. The scanning direction was selected by reconnecting the active elements of the transducer.

An auxiliary ultrasound scanner Medison SA-8000 EX (South Korea), which does not provide access to raw data, was used to control the reliability of observations. This scanner was with used a linear L5-9EC transducer and a convex C3-7ED transducer. The use of the control machine ensured that the artifact appeared as a result of objective physical processes occurring in the examined objects. This reduces the probability of situations in which the twinkling artifact results not from the properties of the object under investigation but from some unknown features of one of the devices.

Principles of CFM Data Acquisition

The size of the CFM area was determined interactively by the examiner. Each direction (beam) in the selected area was sonified N times. A group of N signals obtained by sonifying the same area of tissue is called a Doppler pulse train. The time within the pulse train is called “slow” time, it is measured for a single spatial position, as opposed to the “fast” time, which is directly proportional to the depth. Blood flow and other processes are tracked by changes in “slow” time signals within a single pulse train. If there are no changes in the examined object, these signals are

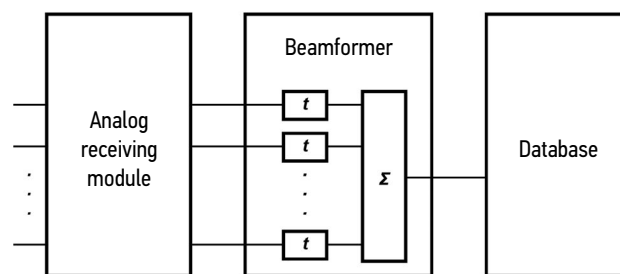


Fig. 1. Data capture scheme.

almost identical, the slight difference is the contribution of the noise.

If the same direction is sonified sequentially to obtain a pulse train, a pulse repetition rate of approximately 5 kHz may be obtained, which is not appropriate for most medical applications. To reduce the pulse repetition rate, the examined area was divided into S scanning subareas (*sweeps*), each of which consisted of M beams (Fig. 2). When obtaining a pulse train, the beams of one subarea were sequentially irradiated from the 1st to the M -th beam. Thus, Doppler pulse trains were formed in parallel for M beams of one subarea. Subsequently, the process was repeated for other subareas, whereas the pulse repetition rate was decreased by M times.

The total size of the range of interest determined the number of beams ($S \times M$). One beam consisted of P complex samples. The Q beam density was sometimes changed to increase the frame rate. Thus, if $Q = 2$, the CFM window was updated twice as fast; however, the information about every second beam was lost.

All these steps were repeated F times; thus, a cine loop was formed, which consisted of F frames. The received signals were recorded in a binary file, and the scanning parameters were placed in a text file of the same name (Table).

Examined objects and observations

Most of the items in the database contain signals that were reflected from objects on which a twinkling artifact is

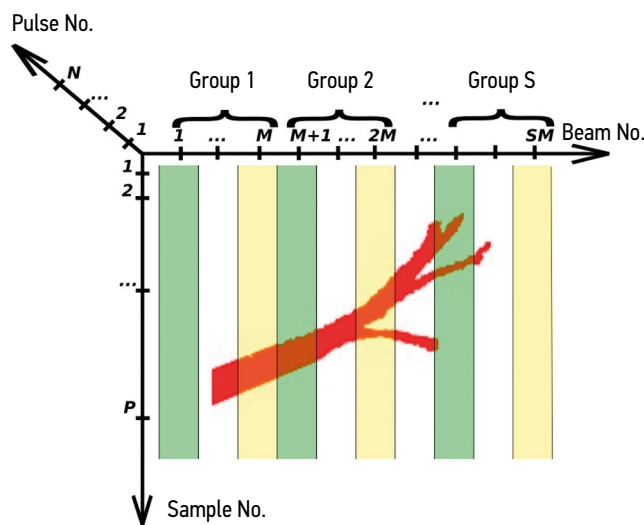


Fig. 2. Explanation of the scanning scheme in the color flow mapping mode. The color coding of the vertical bars corresponds to the number of the beam in the sweep. Red color shows the examined vessel.

observed in Doppler modes. Artificial objects included rough and smooth wire made of low carbon raw steel, and rods made of plastic (ABS), aluminum, and wood. The objects were placed in fixed positions in the body of a specially designed phantom. The body was filled with agar-agar, water, and ethyl alcohol. A Doppler phantom Gammex 1430 LE Mini-Doppler Flow System (USA) was used to record signals from the flowing fluid.

Table. Main scanning parameters displayed in the .par file

Parameters	Description	Symbols
Number of frames	Number of frames	F
Raw frame size	Memory size in bytes occupied by the RF data that is required to build one frame in the duplex B+CFM mode	-
Header size	Memory size in bytes that is reserved in front of each beam	-
Number of B-beams	Number of beams that are used to obtain a gray-scale image	B
Size of B-beam in samples	Number of samples that are used when obtaining a gray-scale image, which depends on the scanning depth	G
Number of CF shots	Number of pulses in a Doppler pulse train	N
Number of sweeps	Number of beam groups in the CFM mode. A group of beams is called a <i>sweep</i> . The CFM-frame consists of several sweeps	S
Beams in sweep	Number of beams in each sweep	M
Size of CFM beam in samples	Number of samples in the CFM mode	P
First scan CFM beam	CFM window position by B-image width	-
CFM density	Beam density in the CFM mode is determined by the formula $(b-a)/c$, where a and b are the numbers of B-beams, which define the left and right borders of the CFM window, and c is the number of CFM beams	Q
Number of CFM beams	Number of beams in the CFM mode	$S \times M$
Number of first CFM sample	Depth position of the CFM window relative to the B-image	-

Note. CFM, color flow mapping.

The Doppler pulse train consisted of 5, 9, or 17 pulses. Examinations with a linear transducer were conducted at a carrier frequency of 7.5 MHz and a power of 74% for B-mode. For the CFM mode, the carrier frequency, power, and pulse repetition rate were 6.3 MHz, 97%, and 750 Hz, respectively. Examinations with a convex transducer were conducted at a carrier frequency and power of 3.3 MHz and 95% in B-mode and 3.3 MHz and 98%, respectively, with a pulse repetition rate of 1 kHz, in the CFM mode. The sampling rate in all cases was 10 MHz. Other settings, such as interframe averaging and wall filter settings, did not affect the data, since the data were obtained from the preprocessing path.

Database contents

Summary of database contents

Records of digital RF signals with twinkling artifact features were collected and placed in the public domain (https://mosmed.ai/datasets/ultrasonic_doppler_twinkling_artifact). The database also contains signals from areas with vessels in the Gammex phantom, specialized phantoms of proprietary design, and reflections from tissue-imitating materials. This database will be useful to researchers who study algorithms for B-mode and CFM signal processing.

The database includes five sets of examinations, which differ in the object of study (Fig. 3). Each examination is a pair of files with the same name and .dat and .par extensions. "Raw" data records are accompanied by images and videos that illustrate the appearance of the twinkling artifact. The examined objects and environments are specified in the directory names of the database. In the directory name, the word "linear" indicates the use of the 7.5 L38 linear

transducers, while "convex" indicates the use of the 3.4 C60 convex transducers.

Database file format

RF signals were recorded in binary form in a file with .dat extension (Fig. 4). This file contained complex data for building a frame in the B-mode (*B-frame*) and CFM mode (*CFM-frame*). The real and imaginary parts of each dataset were written in a "32-bit little-endian (LE) signed integer" format. Initially, a 20-bit header was recorded, which is denoted in Fig. 4 as *H* symbol. Afterward, the samples of the first beam of the B-image, which are denoted as *B-sample 1 to B*, the header, and the samples of the second and subsequent beams of the B-image were recorded.

Then, the samples for constructing the CFM, which are denoted as a *CFM-sample*, were recorded. In this case, the *H* header was recorded first, followed by recording all depth samples, which are obtained for the first pulse in the pulse train and the first beam from the first group (*sweep*). Thus, we obtained the first line of the CFM data; each subsequent line was also separated by a header.

The second and subsequent frames were recorded in the same way. Each .dat file corresponded to a text file of the same name with the .par extension, which contained information on scanning parameters (Table) and specific *F*, *G*, *B*, *F*, *S*, *N*, *M*, *P*, and *Q* values.

Database viewer

The TwinklingDatasetDisplay program is developed to view and analyze the proposed database. The program

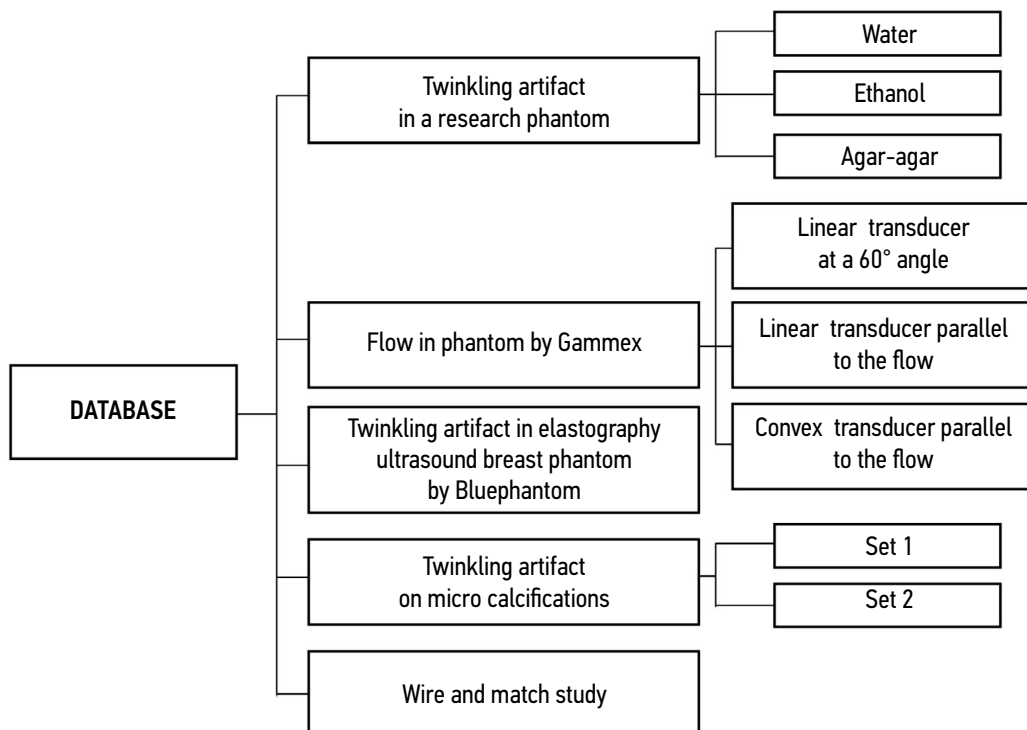


Fig. 3. Composition of the database.

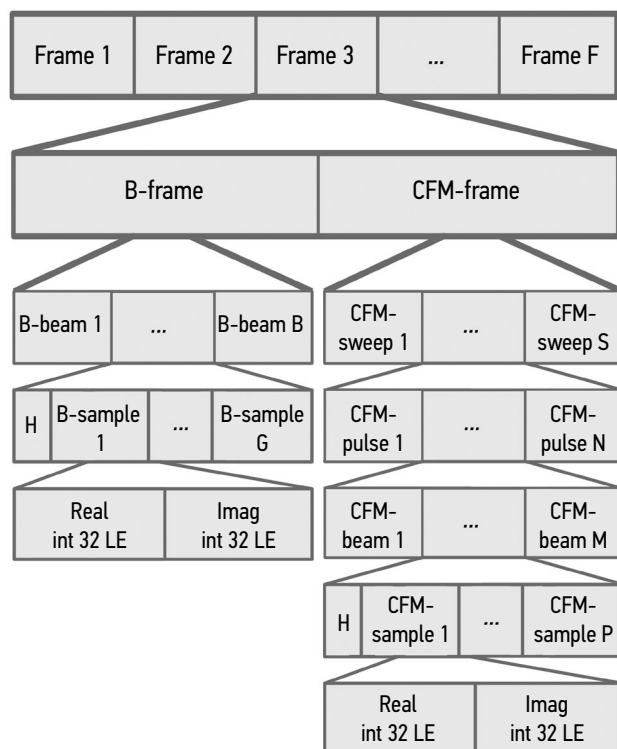


Fig. 4. Scheme for storing “raw” radio frequency data in a *.dat file.

is intended only for viewing RF signals and does not include any signal processing algorithms for CFM [17–30]. All software modules are written in C++ using the XRAD library [31]. The program is in the public domain (<https://github.com/Center-of-Diagnostics-and-Telemedicine/TwinklingDatasetDisplay.git>). The database also included Windows executable files.

The TwinklingDatasetDisplay program allows the following:

- Opening .dat files using information from the .par files.
- Forming a conventional B-mode image from the data.
- Displaying complex signals in the form of graphs depending on both “fast” and “slow” time of the CFM mode.
- Applying elements of spectral analysis thereto.

Examples of “slow” time signals, which determine the Doppler pattern, are shown in Fig. 5. Typical graphs of signals from different areas are shown here:

- The area of the blood-mimicking fluid flow in the Doppler phantom channel of the Gammex 1430 LE Mini-Doppler Flow System (real and imaginary parts of the signal change in quadrature, which is typical for moving objects; Fig. 5a).
- The area of soft tissues in the absence of motion (after filtering the signal from the tissues, only the noise remains; Fig. 5b).
- The observation area of the twinkling artifact on a steel wire (a random signal is observed, which differs from the noise in Fig. 5b by greater dispersion; Fig. 5c).

- The observation area of the twinkling artifact on a smooth object (the signal shows a periodicity resulted from micro-oscillations of the observed object; Fig. 5d).

Database composition

1. A set of examinations of the Gammex 1430 LE Mini-Doppler Flow System.

Fig. 6 shows the external view and scheme of the phantom, and Fig. 7 shows examples of sonograms. In transverse scanning, the linear transducer was positioned at an angle of 60° to the vessel, the flow rate was 30 cm/s, data were obtained at 5, 9, and 17 pulses in train, and the pulse repetition frequency was 2.5 kHz. Concurrently, an observed sonogram in the phantom was very much alike that of the *in vivo* carotid artery.

In the course of longitudinal scanning with a linear transducer, the flow velocity was set to 50 cm/s, and the study was conducted with 17 probing pulses and a frequency of 1 kHz. The velocity projection, which was displayed in the Doppler mode, was close to zero. Such a study may be useful for debugging mapping algorithms.

Longitudinal scanning with a convex transducer was also performed, while three examinations were conducted at different flow rates (i.e., 30 cm/s, 65 cm/s, and 100 cm/s) at a pulse repetition frequency of 2 kHz. For these examinations, a convex transducer was used. The estimated value of the flow velocity projection along a horizontal vessel varied from a negative value, passing through zero, to a positive value; the vessel was colored in the whole palette of the CFM mode.

In Fig. 7 and all subsequent sonograms, both the B-image with the superimposed CFM imaging and the B-image without CFM are placed side by side. Subsequent examinations were conducted using a linear transducer, since it is commonly used in small depth examinations. Preference was given to small values of the pulse repetition frequency since both types of twinkling artifact signals be registered in this case [32].

2. A set of examinations of the custom phantom (Fig. 8; a detailed description of the phantom is available in [32]).

In the phantom study, the linear transducer was applied in fixed numbered positions. Cylinders, with a diameter of 1.75 mm, made of metal (positions 1, 4, and 8), plastic (positions 2, 5, and 7), and wooden rods (positions 3 and 6) in various media (water, alcohol, and agar-agar) were assessed. The set contains examinations that were conducted using a linear transducer at nine probing pulses and a pulse repetition rate of 1 kHz. Typical sonograms are shown in Fig. 9. If the phantom was filled with ethanol, the twinkling artifact was manifested much less frequently in contrast to other media used. In water, the artifact was also noticeable on the air bubbles that rose from the wooden rod. In addition, the twinkling intensity on aluminum rods was noticeably greater than that on plastic and wooden rods.

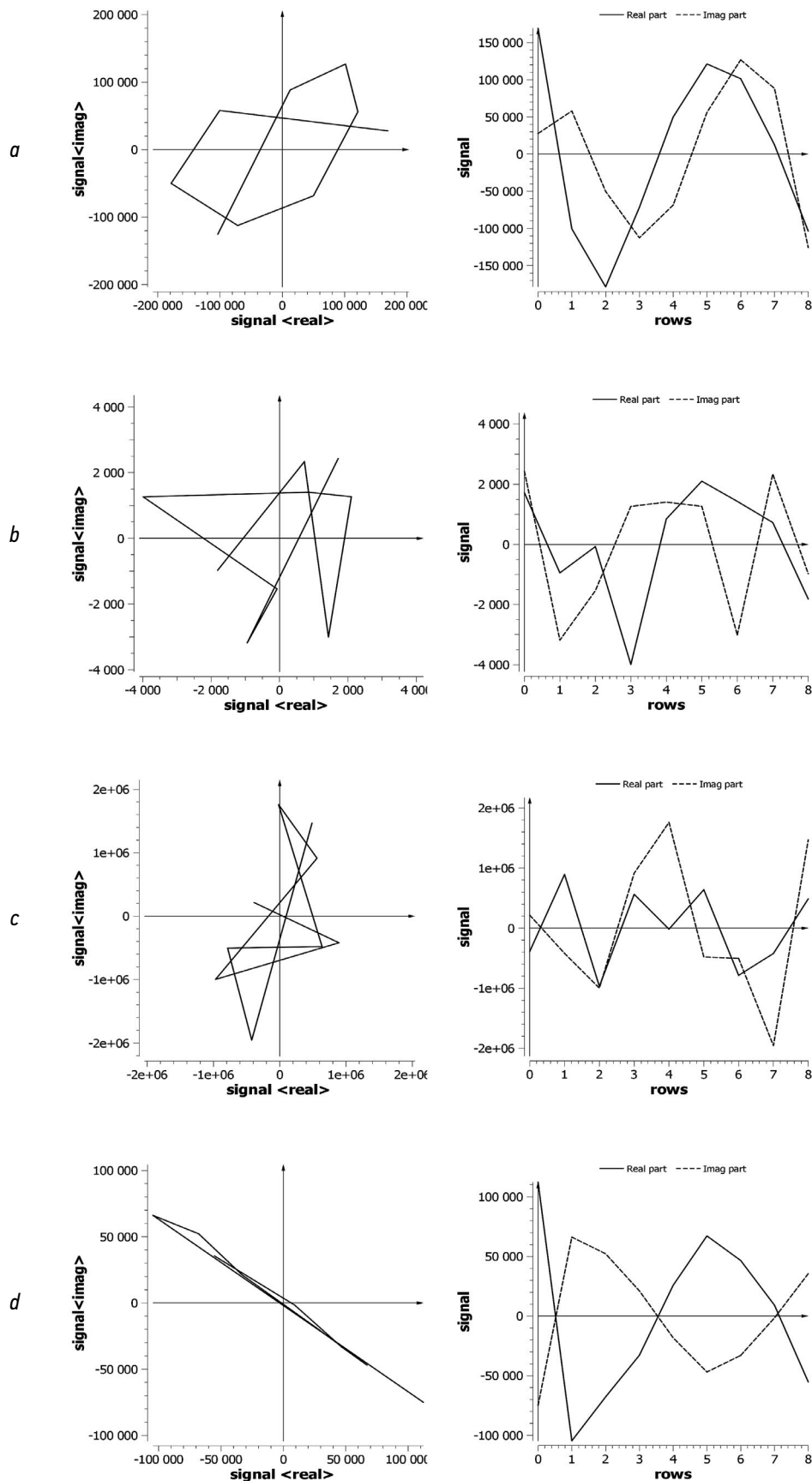


Fig. 5. Examples of visualization of radiofrequency signals using the TwinklingDatasetDisplay program: *a*, fluid flow in the Gammex phantom; *b*, soft tissue area in the absence of motion; *c*, twinkling artifact signal on a rough object; *d*, twinkling artifact signal on a smooth object. In the left column, the complex signals are represented as a parametric line in polar coordinates (the real and imaginary parts are shown on the abscissa and ordinate axes, respectively). The right column shows the dependence on the "slow" time within a pulse train.

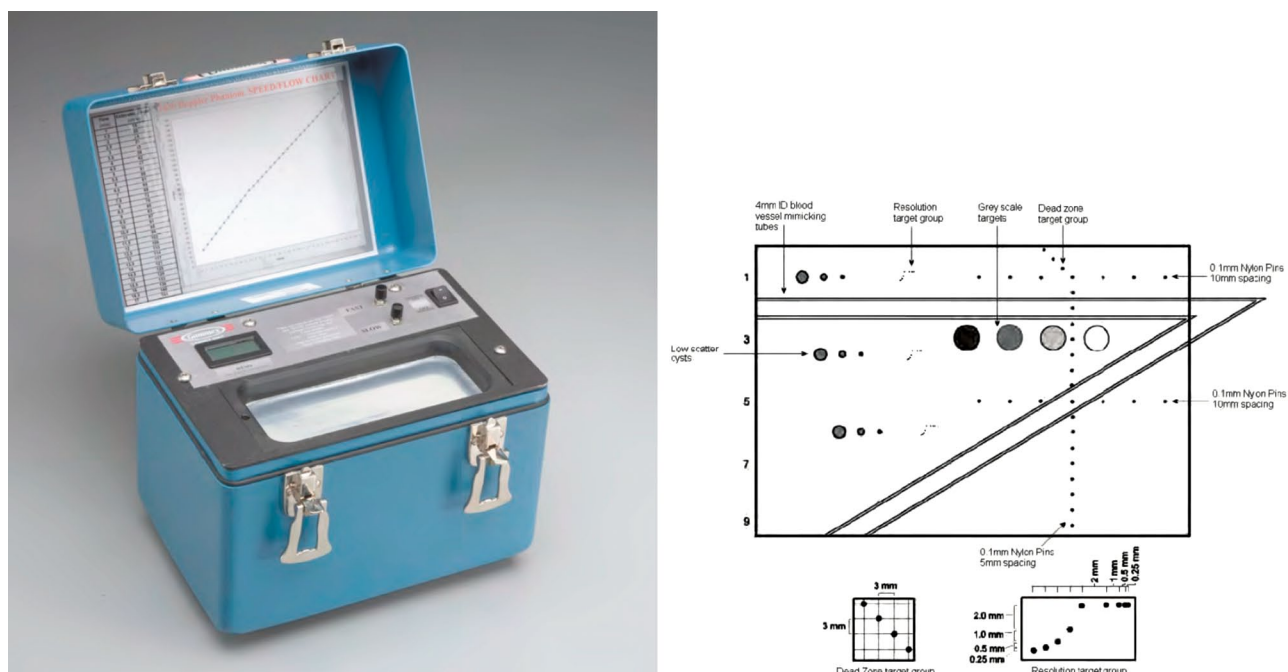


Fig. 6. External view and scheme of the Gammex 1430 LE Mini-Doppler phantom.

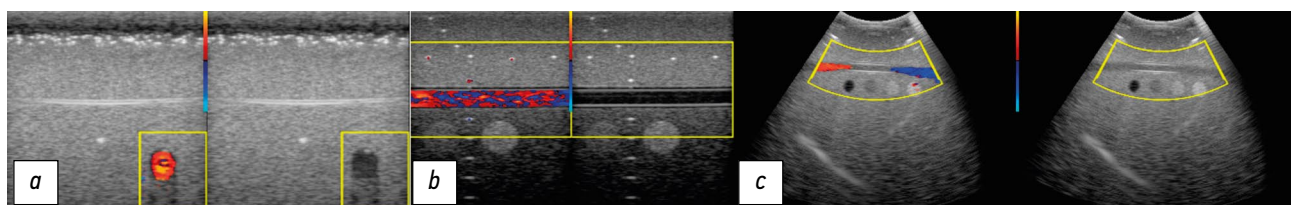


Fig. 7. Sonograms of the Gammex phantom: *a*, examination with a linear sensor at a 60° angle to the flow; *b*, parallel to the flow; *c*, examination with a convex sensor.

3. A set of examinations of elastographic breast Blue Phantom with the data that have been taken with a linear transducer at 5, 9, and 17 pulses in sequence for a pulse repetition frequency of 150 Hz and at 17 pulses and repetition frequencies of 300 Hz, 500 Hz, 750 Hz, and 1 kHz.

The phantom (photo and scheme shown in Fig. 10 *a, b*) contains inclusions that simulate micro calcifications, which are indicated by an arrow in a slice of the computer tomogram in Fig. 10c. On these inclusions, a twinkling artifact was observed at a low pulse repetition frequency in the CFM mode (Fig. 10d). With increasing frequency, the intensity of the artifact decreased until it completely disappeared at frequencies above 1 kHz.

4. A set of approximately 200- μ m micro calcifications that were artificially grown in agar-agar jelly.

Two samples were examined with a linear sensor at a repetition rate of 500 Hz with nine pulses per pulse train. Typical sonograms are shown in Fig. 11.

5. A study of a steel rough wire and a wooden rod in agar-agar jelly.

The study was conducted with a linear transducer at nine pulses. In contrast to the experiment presented in Fig. 9, the

wood was subjected to prolonged pre-wetting and degassing. Both objects produced an acoustic shadow and had the same echogenicity in the B-image (Fig. 12). However, the twinkling artifact appeared on the metal, but not on the wood. The difference in observations allows associating one of the twinkling types with air microbubbles in the wood structure.

Notes on the database use

In most studies [1–8, 10–13], which were devoted to the twinkling artifact, examinations were conducted using commonly available ultrasonic diagnostic devices with no access to the signal processing path. The ultrasonic device can be considered a “black box” in such examinations, and the analysis based only on sonograms on the device screen was not informative enough and created problems with reproducibility, since the algorithms of processing devices of different manufacturers are unique.

Collection of raw data is a prerequisite for developing new ultrasonic imaging tools. However, RF signals from the processing path are commonly not available because of the closed architecture of commercial

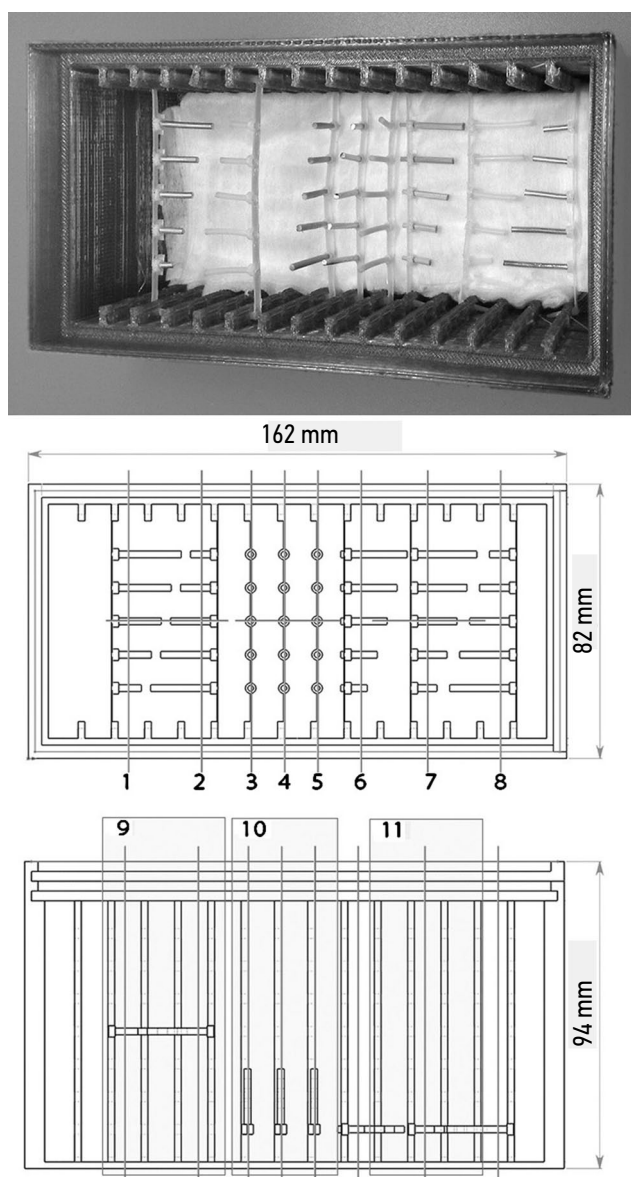


Fig. 8. Photo and drawings of the specialized phantom with dimensions in millimeters and measurement positions.

instruments. A previous study [33] demonstrated a possible solution to this problem, which required a manual modification of the equipment. The proposed database provides all information on signals without the need for self-modification of the commercial equipment with the inevitable loss of warranty and other undesirable consequences.

The proposed database may have great practical value, since it allows the creation of new tools [17] for the detection of kidney stones and other objects, which are associated with a twinkling artifact.

Using the database, we conducted several examinations, as shown below:

- 1) The signals of the twinkling artifact and blood flow were differentiated and two physical causes of the twinkling artifact were investigated. The image on the device screen looks the same; however, different physical

processes are involved therein, which are visible at the signal level [32].

- 2) A special mode was developed, which allowed displaying twinkling not as a Doppler error, which happens to be useful, but as a special diagnostic option [17, 34]. Using this mode, the twinkling may be “pulled out” where a conventional device will not show this artifact. Twinkling and blood flow may be displayed separately or together using different color scales.
- 3) A comparative analysis of filtration algorithms for vessel wall motion (*wall filters*) was conducted [35, 36]. New filtering algorithms appeared in the literature [37–40], their fresh review and comparative analysis are in demand and can be done using our database.

In the future, we would like to complement the database with *in vivo* signals as well as signals that were obtained in other modes (e.g., spectral Doppler mode and vector flow).

Although the program that we designed for opening the database has a minimal set of options, its open-source C++ code allows plentiful modifications. Moreover, the given in this article description gives sufficient information for opening of the database in any programming environment.

Disadvantages of the database

Among the disadvantages of the proposed database, the most significant is the incompleteness of the following information:

- On the examined objects (e.g., only the approximate size of calcinates that were grown in agar jelly was known, the geometrical parameters of the rough wire surface were not investigated).
- On the experimental conditions (in some examinations, the exact position of the transducer, focal distance, and emission power were not recorded; the information on the pulse repetition frequency is not always available).

Code availability

The source code of the program (<https://github.com/Center-of-Diagnostics-and-Telemedicine/TwinklingDataset-Display.git>) is available.

Terms of use

The article presents a database, which contains digital records of raw RF signals from the preprocessing path of the Sonomed-500 ultrasonic device. The database with a total volume of 10.5 Gb contains mostly examinations of objects with a twinkling artifact in the CFM mode. The most obvious application of the database is the development and testing of algorithms for signal processing. The database is publicly available on the Internet under the Creative Commons Attribution – Noncommercial – Share Alike (CC BY-NC-SA) license (https://mosmed.ai/datasets/ultrasonic_doppler_twinkling_artifact).

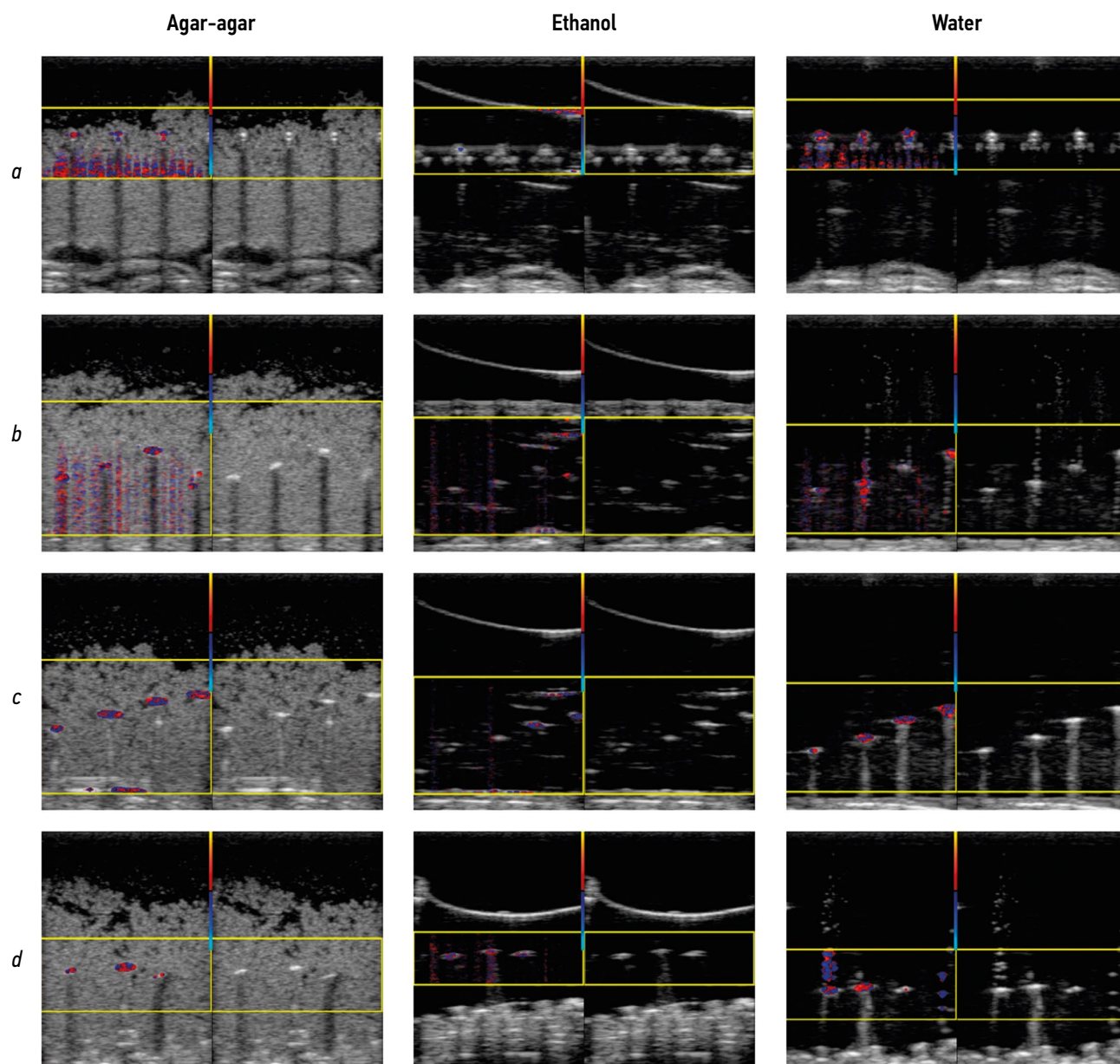


Fig. 9. Examples of sonograms of a specialized phantom with positions and a filling medium: *a*, position 2 (four plastic rods, which are located parallel to the sensor plane); *b*, position 3 (four wooden rods with their sides facing the sensor); *c*, position 4 (four aluminum rods with their sides facing the sensor); *d*, position 10 (wood, aluminum, and plastic rods with their sides facing the sensor).

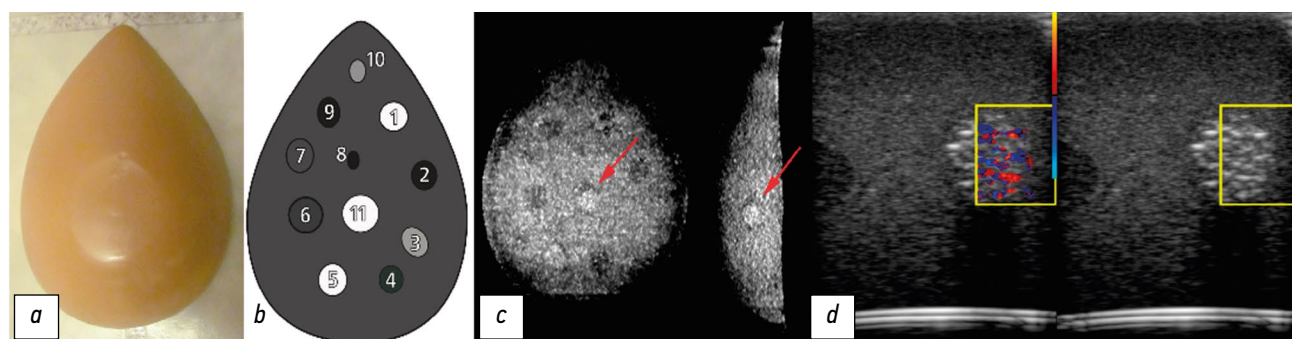


Fig. 10. Blue phantom mammary gland: *a*, external view; *b*, connection scheme; *c*, slices of computed tomogram (the arrow indicates the examined area); *d*, sonogram.

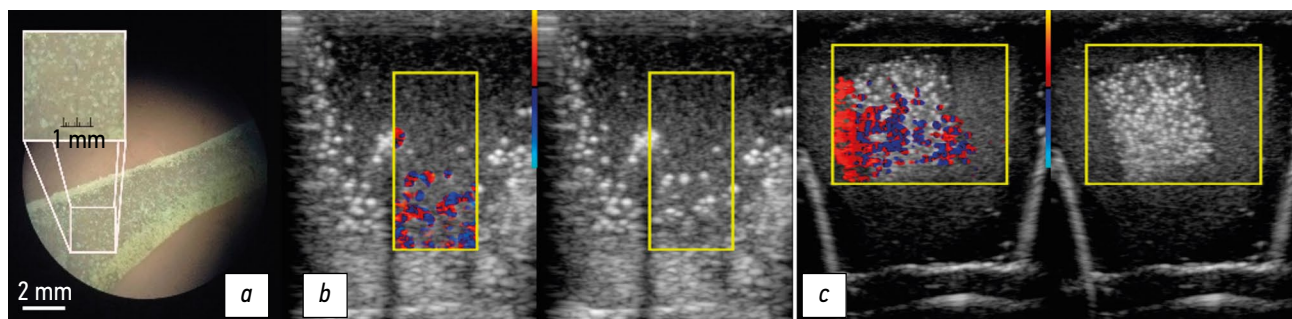


Fig. 11. Sonograms of phantoms with microcrystals that were grown in agar-agar jelly: *a*, sample slice under a microscope; *b*, microcrystals in the growth process; *c*, insertion with microcrystals in the agar-agar phantom.

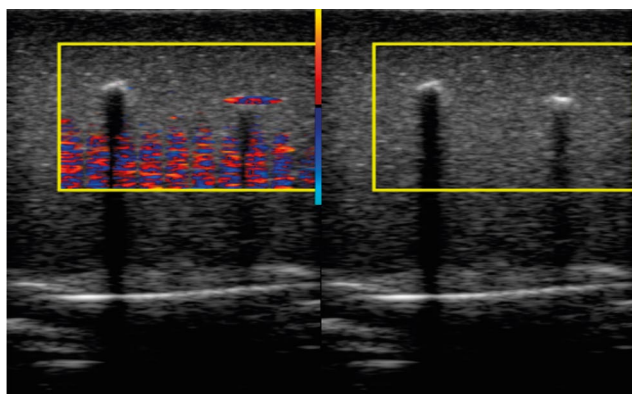


Fig. 12. Sonogram of a phantom with a wooden rod (left) and a steel wire (right).

In case of publication of results that were obtained using the database, please refer to this article. The derivative products must be distributed under the same license. Any attempt to gain financial benefit from the use of the database is strictly prohibited.

REFERENCES

- Masch WR, Cohan RH, Ellis JH, et al. Clinical effectiveness of prospectively reported sonographic twinkling artifact for the diagnosis of renal calculus in patients without known urolithiasis. *Am J Roentgenol.* 2016;206:326–331. doi: 10.2214/ajr.15.14998
- Fujimoto Y, Shimono C, Shimoyama N, Osaki M. Twinkling artifact of microcalcifications in breast ultrasound. *Ultrasound Med Biol.* 2017;43(Suppl. 1):S21. doi: 10.1016/j.ultrasmedbio.2017.08.1010
- Bennett J.M., Estrada J.C., Shoemaker M.B., Pretorius M. Twinkling Artifact Associated with Guidewire Placement. *Anesth Analg.* 2015;121(1):69–71. doi: 10.1213/ane.0000000000000683
- Sen V, Imamoglu C, Kucukturkmen I, et al. Can Doppler ultrasonography Twinkling artifact be used as an alternative imaging modality to non-contrast-enhanced computed tomography in patients with ureteral stones? A prospective clinical study. *Urolithiasis.* 2017;45(2):215–219. doi: 10.1007/s00240-016-0891-8
- Winkel RR, Kalhauge A, Fredfeldt KE. The usefulness of ultrasound colour-Doppler twinkling artefact for detecting urolithiasis compared with low dose nonenhanced computerized tomography.

ADDITIONAL INFORMATION

Funding source. This article was prepared with the support of Moscow Healthcare Department as a part of Program “Scientific Support of the Capital’s Healthcare” for 2020–2022 (Unified State Information System for Accounting of Research, Development, and Technological Works No. AAAA-A20-120071090054-9).

Competing interests. The authors declare that they have no competing interests.

Authors’ contribution. Kulberg N.S. and Leonov D.V. — research concept and design, data collection and processing, preparation of illustrations, and writing the text of the manuscript.

Reshetnikov R.V. and Nasibullina A.A. — participation in the formation of the research plan and discussion each chapter of the manuscript, checking the database, and preparing illustrations.

Gromov A.I. — research concept and design, and manuscript editing. All authors confirm the compliance of the authors with the international ICMJE criteria. All authors made a significant contribution to the development of the concept, research, and preparation of the article, read and approved the final version before publication.

Ultrasound Med Biol. 2012;38(7):1180–1187. doi: 10.1016/j.ultrasmedbio.2012.03.003

6. Yavuz A, Ceken K, Alimoglu E, Kabaalioglu A. The reliability of color Doppler “twinkling” artifact for diagnosing millimetrical nephrolithiasis: comparison with B-Mode US and CT scanning results. *J Med Ultrasonics.* 2015;42(2):215–222. doi: 10.1007/s10396-014-0599-8

7. Tian J, Xu L. Color Doppler Twinkling artifact in diagnosis of tuberculous pleuritis: A comparison with gray-scale ultrasonography and computed tomography. *Ultrasound Med Biol.* 2018;44(6):1291–1295. doi: 10.1016/j.ultrasmedbio.2018.01.003

8. Relea A, Alonso JA, González M, et al. Usefulness of the twinkling artifact on Doppler ultrasound for the detection of breast microcalcifications. *Radiologia.* 2018;60(5):413–423. doi: 10.1016/j.rx.2018.04.004

9. Lu W, Sapozhnikov OA, Bailey MR, et al. Evidence for trapped surface bubbles as the cause for the twinkling artifact in ultrasound imaging. *Ultrasound Med.* 2013;39(6):1026–1038. doi: 10.1016/j.ultrasmedbio.2013.01.011

10. Aytac SK, Ozcan H. Effect of color Doppler system on the «twinkling» sign associated with urinary

- tract calculi. *J Clin Ultrasound*. 1999;27(8):433–439. doi: 10.1002/(sici)1097-0096(199910)27:8<433::aid-jcu4>3.0.co;2-1
11. Rahmouni A, Bargoin R, Herment A, et al. Color Doppler Twinkling artifact in hyperechoic regions. *Radiology*. 1996;199(1):269–271. doi: 10.1148/radiology.199.1.8633158
12. Kamaya A, Tuthill T, Rubin JM. Twinkling artifact on color Doppler sonography: dependence on machine parameters and underlying cause. *Am J Roentgenol*. 2003;180(1):215–222. doi: 10.2214/ajr.180.1.1800215
13. Weinstein SP, Seghal C, Conant EF, Patton JA. Microcalcifications in breast tissue phantoms visualized with acoustic resonance coupled with power doppler US: initial observations. *Radiology*. 2002;224(1):265–269. doi: 10.1148/radiol.2241010511
14. Seghal C. Apparatus for imaging an element within a tissue and method therefor. *United States Patent*. 1999;477(5):997.
15. Li T, Khokhlova TD, Sapozhnikov OA, et al. A new active cavitation mapping technique for pulsed HIFU applications—bubble Doppler. *IEEE Trans Ultrason Ferroelectr Freq Control*. 2014;61(10):1698–1708. doi: 10.1109/TUFFC.2014.006502
16. Simon JC, Sapozhnikov OA, Kreider W, et al. The role of trapped bubbles in kidney stone detection with the color Doppler ultrasound twinkling artifact. *Phys Med Biol*. 2018;63(2):025011. doi: 10.1088/1361-6560/aa9a2f
17. Leonov DV, Kulberg NS, Gromov AI, et al. Diagnostic mode detecting solid mineral inclusions in medical ultrasound imaging. *Acoust Phys*. 2018;64(5):624–636. doi: 10.1134/S1063771018050068
18. Yu AC, Johnston KW, Cobbold RS. Frequency-based signal processing for ultrasound color flow imaging. *Canadian Acoustics*. 2007;35(2):11–23.
19. Yu AC, Løvstakken L. Eigen-based clutter filter design for ultrasound color flow imaging: a review. *IEEE Trans Ultrason Ferroelectr Freq Control*. 2010;57(5):1096–1111. doi: 10.1109/TUFFC.2010.1521
20. Yu AC, Cobbold RS. Single-ensemble-based eigen-processing methods for color flow imaging — Part I. The Hankel-SVD filter. *IEEE Trans Ultrason Ferroelectr Freq Control*. 2008;55(3):559–572. doi: 10.1109/TUFFC.2008.682
21. Shen Z, Feng N, Shen Y, Lee CH. An improved parametric relaxation approach to blood flow signal estimation with single-ensemble in color flow imaging. *J Med Biomed Engineering*. 2013;33(3):309–318. doi: 10.5405/jmbe.1368
22. Yoo YM, Managuli R, Kim Y. Adaptive clutter filtering for ultrasound color flow imaging. *Ultrasound Med Biol*. 2003;29(9):1311–1320. doi: 10.1016/S0301-5629(03)01014-7
23. Torp H. Clutter rejection filters in color flow imaging: a theoretical approach. *IEEE Trans Ultrason Ferroelectr Freq Control*. 1997;44(2):417–424. doi: 10.1109/58.585126
24. Wang PD, Shen Y, Feng NZ. A novel clutter rejection scheme in color flow imaging. *Ultrasonics*. 2006;44(Suppl 1):e303–305. doi: 10.1016/j.ultras.2006.06.017
25. Bjærum S, Torp H. Statistical evaluation of clutter filters in color flow imaging. *Ultrasonics*. 2000;38(1-8):376–380. doi: 10.1016/S0041-624X(99)00153-5
26. Kargel C, Hoebenreich G, Plevnik G, et al. Velocity estimation and adaptive clutter filtering for color flow imaging. *WSEAS*. 2002. P. 1711–1716.
27. Kargel C, Höbenreich G, Trummer B, Insana MF. Adaptive clutter rejection filtering in ultrasonic strain-flow imaging. *IEEE Trans Ultrason Ferroelectr Freq Control*. 2003;50(7):824–835. doi: 10.1109/tuffc.2003.1214502
28. Lo MT, Hu K, Peng CK, Novak V. Multimodal pressure flow analysis: application of hilbert huang transform in carabral blood flow regulation. *EURASIP J Adv Signal Process*. 2008;2008:785243. doi: 10.1155/2008/785243
29. Gerbands JJ. On the relationships between SVD, KLT and PCA. *Pattern Recognition*. 1981;14:375–381. doi: 10.1016/0031-3203(81)90082-0
30. Løvstakken L. Signal processing in diagnostic ultrasound: algorithms for real-time estimation and visualization of blood flow velocity. Doctoral thesis, norwegian university of science and technology. Trondheim; 2007. Available from: <https://pdfslide.net/documents/signal-processing-in-diagnostic-ultrasound-algorithms-for-real-time-.html>. Accessed: 14.08.2021.
31. XRAD C++ software library. Available from: <https://github.com/Center-of-Diagnostics-and-Telemedicine/xrad.git>. Accessed: 14.08.2021.
32. Leonov DV, Kulberg NS, Gromov AI, et al. Causes of ultrasound doppler twinkling artifact. *Acoust Phys*. 2018;64(1):105–114. doi: 10.1134/S1063771018010128
33. Mari JM, Cachard C. Acquire real-time RF digital ultrasound data from a commercial scanner. *Electronic J Technical Acoustics*. 2007;3:28–43.
34. Leonov DV, Kulberg NS, Gromov AI, Morozov SP. Detection of microcalcifications using the ultrasound Doppler twinkling artifact. *Biomedical Engineering*. 2020;54(3):174–178. doi: 10.1007/s10527-020-09998-y
35. Leonov DV, Kulberg NS, Fin VA, et al. Clutter filtering for diagnostic ultrasound color flow imaging. *Biomedical Engineering*. 2019;53(3):217–221. doi: 10.1007/s10527-019-09912-1
36. Leonov DV, Kulberg NS, Fin VA, et al. Comparison of filtering techniques in ultrasound color flow imaging. *Biomedical Engineering*. 2019;53(2):97–101. doi: 10.1007/s10527-019-09885-1
37. Song P, Manduca A, Trzasko JD, Chen S. Ultrasound small vessel imaging with block-wise adaptive local clutter filtering. *IEEE Trans Med Imaging*. 2017;36(1):251–262. doi: 10.1109/TMI.2016.2605819
38. Li YL, Hyun D, Abou-Elkacem L, et al. Visualization of small-diameter vessels by reduction of incoherent reverberation with coherent flow power doppler. *IEEE Trans Ultrason Ferroelectr Freq Control*. 2016;63(11):1878–1889. doi: 10.1109/TUFFC.2016.2616112
39. Chee AJ, Alfred CH. Receiver operating characteristic analysis of eigen-based clutter filters for ultrasound color flow imaging. *IEEE Trans Ultrason Ferroelectr Freq Control*. 2017;65(3):390–399. doi: 10.1109/TUFFC.2017.2784183
40. Chee AJ, Yiu BY, Alfred CH. A GPU-Parallelized eigen-based clutter filter framework for ultrasound color flow imaging. *IEEE Trans Ultrason Ferroelectr Freq Control*. 2017;64(1):150–163. doi: 10.1109/TUFFC.2016.2606598

СПИСОК ЛИТЕРАТУРЫ

1. Masch W.R., Cohan R.H., Ellis J.H., et al. Clinical effectiveness of prospectively reported sonographic twinkling artifact for the diagnosis of renal calculus in patients without known urolithiasis // *Am J Roentgenol.* 2016. Vol. 206. P. 326–331. doi: 10.2214/ajr.15.14998
2. Fujimoto Y., Shimono C., Shimoyama N., Osaki M. Twinkling artifact of microcalcifications in breast ultrasound // *Ultrasound Med Biol.* 2017. Vol. 43, Suppl. 1. P. S21. doi: 10.1016/j.ultrasmedbio.2017.08.1010
3. Bennett J.M., Estrada J.C., Shoemaker M.B., Pretorius M. Twinkling artifact associated with guidewire placement // *Anesth Analg.* 2015. Vol. 121, N 1. P. 69–71. doi: 10.1213/ane.0000000000000683
4. Sen V., Imamoglu C., Kucukurkmen I., et al. Can Doppler ultrasonography Twinkling artifact be used as an alternative imaging modality to non-contrast-enhanced computed tomography in patients with ureteral stones? A prospective clinical study // *Urolithiasis.* 2017. Vol. 45, N 2. P. 215–219. doi: 10.1007/s00240-016-0891-8
5. Winkel R.R., Kalhauge A., Fredfeldt K.E. The usefulness of ultrasound colour-Doppler twinkling artefact for detecting urolithiasis compared with low dose nonenhanced computerized tomography // *Ultrasound Med Biol.* 2012. Vol. 38, N 7. P. 1180–1187. doi: 10.1016/j.ultrasmedbio.2012.03.003
6. Yavuz A., Ceken K., Alimoglu E., Kabaalioglu A. The reliability of color Doppler "twinkling" artifact for diagnosing millimetrical nephrolithiasis: comparison with B-Mode US and CT scanning results // *J Med Ultrasonics.* 2015. Vol. 42, N 2. P. 215–222. doi: 10.1007/s10396-014-0599-8
7. Tian J., Xu L. Color Doppler Twinkling artifact in diagnosis of tuberculous pleuritis: A comparison with gray-scale ultrasonography and computed tomography // *Ultrasound Med Biol.* 2018. Vol. 44, N 6. P. 1291–1295. doi: 10.1016/j.ultrasmedbio.2018.01.003
8. Relea A., Alonso J.A., González M., et al. Usefulness of the twinkling artifact on Doppler ultrasound for the detection of breast microcalcifications // *Radiología.* 2018. Vol. 60, N 5. P. 413–423. doi: 10.1016/j.rx.2018.04.004
9. Lu W., Sapozhnikov O.A., Bailey M.R., et al. Evidence for trapped surface bubbles as the cause for the twinkling artifact in ultrasound imaging // *Ultrasound Med.* 2013. Vol. 39, N 6. P. 1026–1038. doi: 10.1016/j.ultrasmedbio.2013.01.011
10. Aytac S.K., Ozcan H. Effect of color Doppler system on the «twinkling» sign associated with urinary tract calculi // *J Clin Ultrasound.* 1999. Vol. 27, N 8. P. 433–439. doi: 10.1002/(sici)1097-0096(199910)27:8<433::aid-jcu4>3.0.co;2-1
11. Rahmouni A., Bargoin R., Herment A., et al. Color doppler twinkling artifact in hyperechoic regions // *Radiology.* 1996. Vol. 199, N 1. P. 269–271. doi: 10.1148/radiology.199.1.8633158
12. Kamaya A., Tuthill T., Rubin J.M. Twinkling artifact on color Doppler sonography: dependence on machine parameters and underlying cause // *Am J Roentgenol.* 2003. Vol. 180, N 1. P. 215–222. doi: 10.2214/ajr.180.1.1800215
13. Weinstein S.P., Seghal C., Conant E.F., Patton J.A. Microcalcifications in breast tissue phantoms visualized with acoustic resonance coupled with power doppler US: initial observations // *Radiology.* 2002. Vol. 4, N 1. P. 265–269. doi: 10.1148/radiol.2241010511
14. Seghal C. Apparatus for imaging an element within a tissue and method therefor // United States Patent. 1999. Vol. 477, N 5. P. 997.
15. Li T., Khokhlova T.D., Sapozhnikov O.A., et al. A new active cavitation mapping technique for pulsed HIFU applications—bubble Doppler // *IEEE Trans Ultrason Ferroelectr Freq Control.* 2014. Vol. 61, N 10. P. 1698–708. doi: 10.1109/TUFFC.2014.006502
16. Simon J.C., Sapozhnikov O.A., Kreider W., et al. The role of trapped bubbles in kidney stone detection with the color Doppler ultrasound twinkling artifact // *Phys Med Biol.* 2018. Vol. 63, N 2. P. 025011. doi: 10.1088/1361-6560/aa9a2f
17. Leonov D.V., Kulberg N.S., Gromov A.I., et al. Diagnostic mode detecting solid mineral inclusions in medical ultrasound imaging // *Acoust Phys.* 2018. Vol. 64, N 5. P. 624–636. doi: 10.1134/S1063771018050068
18. Yu A.C., Johnston K.W., Cobbold R.S. Frequency-based signal processing for ultrasound color flow imaging // *Canadian Acoustics.* 2007. Vol. 35, N 2. P. 11–23.
19. Yu A.C., Løvstakken L. Eigen-based clutter filter design for ultrasound color flow imaging: a review // *IEEE Trans Ultrason Ferroelectr Freq Control.* 2010. Vol. 57, N 5. P. 1096–1111. doi: 10.1109/TUFFC.2010.1521
20. Yu A.C., Cobbold R.S. Single-Ensemble-based eigen-processing methods for color flow imaging — Part I. The Hankel-SVD filter // *IEEE Trans Ultrason Ferroelectr Freq Control.* 2008. Vol. 55, N 3. P. 559–572. doi: 10.1109/TUFFC.2008.682
21. Shen Z., Feng N., Shen Y., Lee C.H. An improved parametric relaxation approach to blood flow signal estimation with single-ensemble in color flow imaging // *J Med Biomed Engineering.* 2013. Vol. 33, N 3. P. 309–318. doi: 10.5405/jmbe.1368
22. Yoo Y.M., Managuli R., Kim Y. Adaptive clutter filtering for ultrasound color flow imaging // *Ultrasound Med Biol.* 2003. Vol. 29, N 9. P. 1311–1320. doi: 10.1016/S0301-5629(03)01014-7
23. Torp H. Clutter rejection filters in color flow imaging: a theoretical approach // *IEEE Trans Ultrason Ferroelectr Freq Control.* 1997. Vol. 44, N 2. P. 417–424. doi: 10.1109/58.585126
24. Wang P.D., Shen Y., Feng N.Z. A novel clutter rejection scheme in color flow imaging // *Ultrasonics.* 2006. Vol. 44, Suppl 1. P. e303–305. doi: 10.1016/j.ultras.2006.06.017
25. Bjærum S., Torp H. Statistical evaluation of clutter filters in color flow imaging // *Ultrasonics.* 2000. Vol. 38, N 1–8. P. 376–380. doi: 10.1016/s0041-624x(99)00153-5
26. Kargel C., Hoebenreich G., Plevnik G., et al. Velocity estimation and adaptive clutter filtering for color flow imaging // *WSEAS.* 2002. P. 1711–1716.
27. Kargel C., Höbenreich G., Trummer B., Insana M.F. Adaptive clutter rejection filtering in ultrasonic strain-flow imaging // *IEEE Trans Ultrason Ferroelectr Freq Control.* 2003. Vol. 50, N 7. P. 824–835. doi: 10.1109/tuffc.2003.1214502
28. Lo M.T., Hu K., Peng C.K., Novak V. Multimodal pressure flow analysis: application of hilbert huang transform in carabral blood flow regulation // *EURASIP J Adv Signal Process.* 2008. Vol. 2008. P. 785243. doi: 10.1155/2008/785243
29. Gerbands J.J. On the relationships between SVD, KLT and PCA // *Pattern Recognition.* 1981. Vol. 14. P. 375–381. doi: 10.1016/0031-3203(81)90082-0

- 30.** Løvstakken L. Signal processing in diagnostic ultrasound: algorithms for real-time estimation and visualization of blood flow velocity. Doctoral thesis, norwegian university of science and technology. Trondheim; 2007. Режим доступа: <https://pdfslide.net/documents/signal-processing-in-diagnostic-ultrasound-algorithms-for-real-time-.html>. Дата обращения: 14.08.2021.
- 31.** XRAD C++ software library. Режим доступа: <https://github.com/Center-of-Diagnostics-and-Telemedicine/xrad.git>. Дата обращения: 14.08.2021.
- 32.** Leonov D.V., Kulberg N.S., Gromov A.I., et al. Causes of ultrasound doppler twinkling artifact // *Acoust Phys*. 2018. Vol. 64, N 1. P. 105–114. doi: 10.1134/S1063771018010128
- 33.** Mari J.M., Cachard C. Acquire real-time RF digital ultrasound data from a commercial scanner // *Electronic J Technical Acoustics*. 2007. Vol. 3. P. 28–43.
- 34.** Leonov D.V., Kulberg N.S., Gromov A.I., Morozov S.P. Detection of microcalcifications using the ultrasound Doppler twinkling artifact // *Biomedical Engineering*. 2020. Vol. 54, N 3. P. 174–178. doi: 10.1007/s10527-020-09998-y
- 35.** Leonov D.V., Kulberg N.S., Fin V.A., et al. Clutter filtering for diagnostic ultrasound color flow imaging // *Biomedical Engineering*. 2019. Vol. 53, N 3. P. 217–221. doi: 10.1007/s10527-019-09912-1
- 36.** Leonov D.V., Kulberg N.S., Fin V.A., et al. Comparison of filtering techniques in ultrasound color flow imaging // *Biomedical Engineering*. 2019. Vol. 53, N 2. P. 97–101. doi: 10.1007/s10527-019-09885-1
- 37.** Song P., Manduca A., Trzasko J.D., Chen S. Ultrasound small vessel imaging with block-wise adaptive local clutter filtering // *IEEE Trans Med Imaging*. 2017. Vol. 36, N 1. P. 251–262. doi: 10.1109/TMI.2016.2605819
- 38.** Li Y.L., Hyun D., Abou-Elkacem L., et al. Visualization of small-diameter vessels by reduction of incoherent reverberation with coherent flow power doppler // *IEEE Trans Ultrason Ferroelectr Freq Control*. 2016. Vol. 63, N 11. P. 1878–1889. doi: 10.1109/TUFFC.2016.2616112
- 39.** Chee A.J., Alfred C.H. Receiver operating characteristic analysis of eigen-based clutter filters for ultrasound color flow imaging // *IEEE Trans Ultrason Ferroelectr Freq Control*. 2017. Vol. 65, N 3. P. 390–399. doi: 10.1109/TUFFC.2017.2784183
- 40.** Chee A.J., Yiu B.Y., Alfred C.H. A GPU-Parallelized eigen-based clutter filter framework for ultrasound color flow imaging // *IEEE Trans Ultrason Ferroelectr Freq Control*. 2017. Vol. 64, N 1. P. 150–163. doi: 10.1109/TUFFC.2016.2606598

AUTHORS' INFO

* **Denis V. Leonov**, Cand. Sci. (Tech);

address: 28-1, Srednyaya Kalitnikovskaya street, Moscow, 109029, Russia;

ORCID: <http://orcid.org/0000-0003-0916-6552>;

eLibrary SPIN: 5510-4075; e-mail: strat89@mail.ru

Roman V. Reshetnikov, Cand. Sci. (Phys.-Math.);

ORCID: <http://orcid.org/0000-0002-9661-0254>;

eLibrary SPIN: 8592-0558; e-mail: reshetnikov@fbb.msu.ru

Nikolay S. Kulberg, Cand. Sci. (Phys.-Math.);

ORCID: <http://orcid.org/0000-0001-7046-7157>;

eLibrary SPIN: 2135-9543; e-mail: kulberg@npcmr.ru

Anastasia A. Nasibullina;

ORCID: <http://orcid.org/0000-0003-1695-7731>;

eLibrary SPIN: 2482-3372; e-mail: nastya.nasibullina@yandex.ru

Alexandr I. Gromov, MD, Dr. Sci. (Med.), Professor;

ORCID: <http://orcid.org/0000-0002-9014-9022>;

eLibrary SPIN: 6842-8684; e-mail: gromov.ai@medsigroup.ru

ОБ АВТОРАХ

* **Леонов Денис Владимирович**, к.т.н.;

адрес: Россия, 109029, Москва,

ул. Средняя Калитниковская, д. 28, стр. 1;

ORCID: <http://orcid.org/0000-0003-0916-6552>;

eLibrary SPIN: 5510-4075; e-mail: strat89@mail.ru

Решетников Роман Владимирович, к.ф.-м.н.;

ORCID: <http://orcid.org/0000-0002-9661-0254>;

eLibrary SPIN: 8592-0558; e-mail: reshetnikov@fbb.msu.ru

Кульберг Николай Сергеевич, к.ф.-м.н.;

ORCID: <http://orcid.org/0000-0001-7046-7157>;

eLibrary SPIN: 2135-9543; e-mail: kulberg@npcmr.ru

Насибуллина Анастасия Александровна;

ORCID: <http://orcid.org/0000-0003-1695-7731>;

eLibrary SPIN: 2482-3372; e-mail: nastya.nasibullina@yandex.ru

Громов Александр Игоревич, д.м.н., профессор;

ORCID: <http://orcid.org/0000-0002-9014-9022>;

eLibrary SPIN: 6842-8684; e-mail: gromov.ai@medsigroup.ru

* Corresponding author / Автор, ответственный за переписку